Mitigating Hallucination in Large Vision-Language Models via Modular Attribution and Intervention

Tianyun Yang[1,2,3] **Ziniu Li**[4] **Juan Cao**[1,2] **Chang Xu**[3]
[1] Institute of Computing Technology, Chinese Academy of Sciences, Beijing, China
[2] University of Chinese Academy of Sciences, Beijing, China
[3] School of Computer Science, Faculty of Engineering, University of Sydney, Australia
[4] School of Data Science, The Chinese University of Hong Kong, Shenzhen
yangtianyun19z@ict.ac.cn, ziniuli@link.cuhk.edu.cn
caojuan@ict.ac.cn, c.xu@sydney.edu.au

Abstract

Large Vision-Language Models (LVLMs) exhibit impressive capabilities in complex visual tasks but are prone to hallucination, especially in open-ended generation tasks. This paper explores why LVLMs tend to hallucinate and how to mitigate it. First, we conduct causal mediation analysis through counterfactual edits on specific modules in LVLMs. Our results disclose that Multi-Head Attention (MHA) modules contribute more to the probability of generating hallucination words than multi-layer perceptron modules. We then identify specific heads that are responsible for hallucination, referred to as hallucination heads. Second, we examine the behavior of hallucination heads. We find that they are concentrated in the middle and deeper layers, displaying a strong attention bias toward text tokens. Further, we show that the attention patterns of certain hallucination heads exhibit greater similarity to the base language model. Finally, we propose two simple yet effective methods to mitigate hallucination: one is training-free and can be applied directly during decoding, while the other involves fine-tuning. Both methods are *targeted* for hallucination heads to reduce their reliance on text tokens. Notably, our methods achieve up to 1.7x reduction in hallucination rate for the LLaVA-v1.5-7B model in COCO captioning task, outperforming existing baselines. Overall, our findings suggest that hallucinations in LVLMs are likely to stem from certain modules, and targeted interventions can effectively mitigate these issues.

1 Introduction

Large Vision-Language Models (LVLMs) [17, 31, 21, 13, 2] have shown impressive performance in tasks ranging from image description to complex reasoning, but they often hallucinate, generating content that deviates from image information, particularly in open-ended tasks like captioning [3]. This highlights a key weakness and risks misleading users. Understanding and mitigating hallucinations is crucial for improving the reliability of these models.

Tracing the causes of hallucinations in LVLMs is difficult due to their complex training pipeline, which combines visual pre-training and instruction tuning on a pre-trained language model [17, 31]. The Transformer-based architecture [22] further complicates interpretation. Studies have found multiple contributing factors: Leng *et al.* [12] showed that visual uncertainty from distorted images amplifies hallucinations, while Huang *et al.* [11] noted that over-reliance on summary tokens neglects key image information. Moreover, Li *et al.* [14] and Zhou *et al.* [30] observed that models hallucinate by generating frequently co-occurring objects inaccurately. See Appendix A for related work.

In this paper, we explore the causes of hallucinations in Large Vision-Language Models (LVLMs), focusing primarily on the LLaVA-v1.5-7B model. In Section 2.1, we identify specific components,

Workshop on Adaptive Foundation Models (NeurIPS 2024).

particularly Multi-Head Attention (MHA) modules in the middle and deeper layers, as key contributors to generating hallucination words. Our analysis in Section 2.2 reveals that hallucination heads prioritize text over visual inputs, inheriting biased attention patterns from the base language model, which remain unchanged after instruction tuning. To mitigate hallucinations, in Section 2.3 we propose two strategies—downscaling text attention weights during decoding and fine-tuning hallucination heads—both of which reduce hallucination rates and outperform existing baselines.

2 Hallucination Attribution and Intervention

2.1 Tracing Hallucination Behaviors to Model Components

The first step in our workflow is selecting a neural network with significant hallucination behaviors, for which we choose LLaVA-7B.[1] We then break the model into smaller units, focusing on MHA (multi-head attention) and MLP (multi-layer perceptron), and use causal mediation analysis via a "knockout" technique [24]. By zero-ablating components, we quantify each one's influence on hallucinations using:

$$\mathcal{I}_c = \frac{1}{m}\sum_{t=1}^{T}\mathbb{I}\left\{y_t \in \text{hallucination}\right\}\left[\mathbb{P}_M(y_t|v,x,y_{<t}) - \mathbb{P}_{M\setminus c}(y_t|v,x,y_{<t})\right] \tag{1}$$

where higher $\mathcal{I}_c$ values indicate greater contribution to hallucination.

For our analysis, we use the COCO dataset [16], sampling 1,500 images from the training set. Following standard practice [11], we prompt the LVLM with the instruction:“Please describe the image in detail." Objects that match the ground truth labels are marked as non-hallucinated, while mismatches are classified as hallucinated. Subsequently, we perform zero-ablation on each MLP and MHA independently, calculate the influence score as in Equation (1), and present the average results for all MLPs and MHAs in Figure 1.

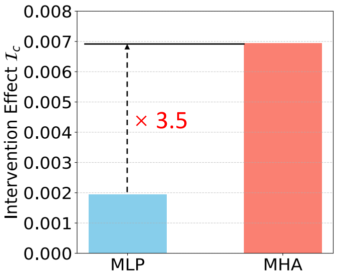

Figure 1: Influence scores of MLP and MHAs in LLaVa-7B on generation probability of hallucination objects.

MHAs have greater effects than MLPs for Hallucination. We observe that removing MLP layers has less impact than MHAs. This finding aligns with [9], which demonstrated that MHAs have a significant effect on classification accuracy in the transformer model CLIP [19]. Intuitively, MHAs focus on capturing relationships and dependencies between tokens through attention weights, whereas MLPs primarily process the information output by MHAs. The differing effects of these interventions suggest that hallucinations often stem from the model's attention to specific patterns or biases, highlighting the need for a more targeted analysis of these components.

Building on our findings, we further investigate attention heads linked to hallucinations. Identifying these heads is challenging due to their polysemantic functionality, as they can influence multiple behaviors simultaneously. To address this, we introduce a new criterion, the **contrastive influence score**, which measures the difference between an attention head's impact on hallucination versus non-hallucination words:

$$\mathcal{I}_{h,\text{constrastive}} = \mathcal{I}_{h,\text{hallucination}} - \mathcal{I}_{h,\text{non-hallucination}}. \tag{2}$$

We apply this score to 1,024 attention heads across 32 layers to identify those most responsible for hallucinations (see Figure 2).

Hallucination Heads Distribute in Middle and Last Layers. For clarity, we categorize attention heads into two groups based on their contrastive influence scores: hallucination heads, which exhibit high contrastive influence score, and non-hallucination heads, which show low contrastive influence score. Rather than using a strict threshold to define these categories, we apply a top-k selection, focusing on heads with the highest and lowest contrastive influence scores. Notably, both hallucination and non-hallucination heads, particularly the most prominent ones (e.g., the top 20 highlighted in boxes in Figure 2), are predominantly located in the middle and deeper layers of the model. This

[1] Our findings also apply to other models, such as MiniGPT4; see Appendix D.1.

finding aligns with previous studies on Transformer models [23], which have shown that deeper layers tend to capture more abstract and task-specific representations.

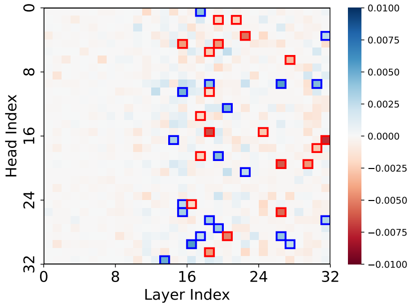

Figure 2: Contrastive influence values of attention heads in the LLaVA-7B model, with blue boxes for the top 20 hallucination heads and red boxes for non-hallucination heads.

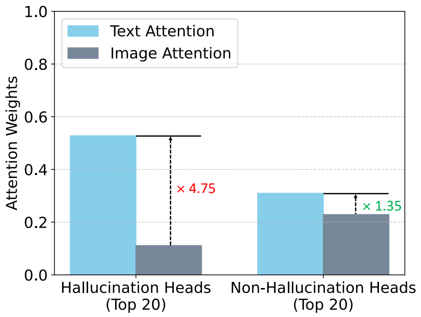

Figure 3: Attention weights on text and image tokens for hallucination and non-hallucination heads. Hallucination heads strongly favor text tokens over image tokens.

2.2 Behaviour Analysis of Hallucination Heads

After attributing attention heads responsible for hallucination in Section 2.1, we analyze their behavior patterns in this section. To understand why they induce hallucinations, we examine their attention maps. In particular, we divide the attention weights of an attention head into two parts: `text attention` and `image attention`. For each attention head, `text attention` is calculated by summing the attention weights assigned to tokens corresponding to instructions and responses[2], while `image attention` is determined by summing the attention weights assigned to tokens representing image features. See Figure 3 for the results.

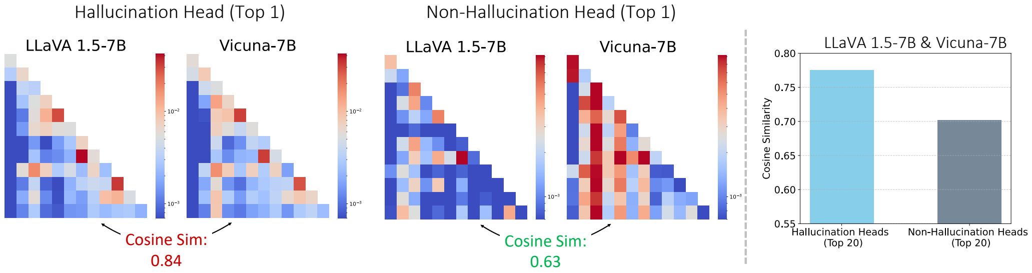

Figure 4: (Left and Middle): Attention maps of the top-1 hallucination heads and non-hallucination heads on generated text tokens of LVLM and its base LLM. Attention maps are downsampled for better visualization. (Right): Statistics over the top-20 attention heads.

Hallucination Heads Favor Texts Over Image Inputs. We observe that for hallucination heads, `text attention` is 4.75 times higher than `image attention`. In contrast, non-hallucination heads allocate attention more evenly between text and images tokens. This suggests that hallucination heads primarily focus on contextual text, causing LVLMs to rely on internal knowledge rather than image inputs when generating relevant words. This behavior helps explain the tendency toward hallucination. Our finding aligns with observations from previous research [12, 11], which also suggest that LVLMs tend to overlook visual information during generation. However, a key difference is that we show this overlooking of visual information primarily occurs in hallucination heads rather than across all attention heads. This insight offers actionable guidance for developing targeted strategies to mitigate hallucinations, as discussed in Section 2.3.

Inherited Attention Patterns in Hallucination Heads from Base Language Models. We also observe a notable similarity in the attention maps on generated text tokens between the hallucination heads of LLaVA-7B and Vicuna-7B, despite Vicuna-7B not processing actual image inputs. In

[2] System tokens are excluded in the calculation here, as they often serve as "attention sink" and lack specific semantic meanings [25]. Thus, the sum of attentions weights in Figure 3 may not be 1.

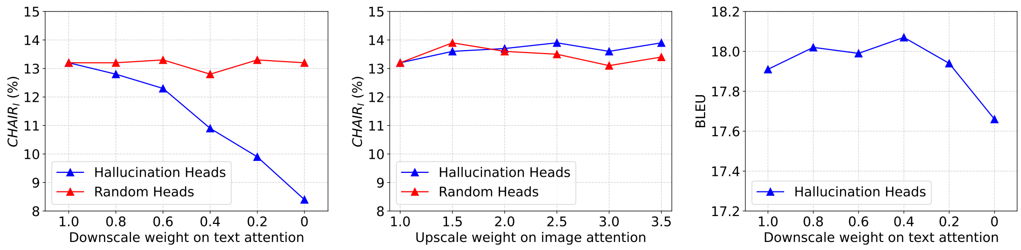

(a) (b) (c)

Figure 5: (a) Downscaling text attention weights reduce hallucination rate. (b) Upscaling image attention weights does not work. (c) Downscaling text attentions weights to zero lead to the drop in generation quality of BLEU.

contrast, non-hallucination heads do not exhibit such a clear pattern, particularly in the most prominent hallucination and non-hallucination heads. See Figure Figure 4 for the results. This suggests that hallucination heads may inherit much of their behavior from the base language model's next-token prediction.

2.3 Mitigating Hallucination through modular intervention

The findings in Section 2.2 lead us to explore a practical question: can hallucination be reduced if attention heads place less emphasis on text tokens, or alternatively, if they place more emphasis on image tokens? To investigate this, we adjust the text generation process by downscaling text attention and upscaling image attention through multiplication by a scaling factor. The results, as presented in Figure 5, offer three interesting insights. First, reducing text attention weights is more effective than increasing image attention weights.[3] Second, targeted intervention of text tokens on hallucination heads is more important than applying changes to the other attention heads. Last, simply downscaling text attention on hallucination heads to zero could hurt generation quality, as reflected in the BLEU score drops in Figure 5 (c).

Based on these insights, we propose two strategies to mitigate hallucination: adaptively deactivate text attention weights during the decoding stage (Section 2.3.1) and fine-tuning hallucination heads to specifically correct their attention patterns (Section 2.3.2).

2.3.1 Adaptive Deactivation of Hallucination Heads

According to results presented in Figure 5, pruning the text attention weights of hallucination heads proves to be an effective decoding-time strategy but at the cost of the quality of text generation, potentially leading to less coherent outputs. To address this, we propose a more adaptive strategy, to deactivate text attention only for those hallucination heads that demonstrate excessive reliance on text attention during the decoding phase.

The adaptive deactivation mechanism works by evaluating each hallucination head $h \in \mathcal{H}_{\text{hallucination}}$ at each decoding step t. We compute the self-attention weights A_h using the softmax of the query-key dot product. To check if the head over-relies on text information, we calculate an indicator I_h^{text} that sums the attention weights on text tokens. If I_h^{text} exceeds a threshold τ, the head is deactivated by setting its text attention weights to zero for that step; otherwise, it remains active. See Algorithm 1 in the Appendix. We would like to note that Algorithm 1 requires a single generation forward process in the decoding stage. This differs from contrastive decoding methods [6, 12], which require two passes, or methods [11, 30] that rely on beam search and retrospection. As a result, Algorithm 1 runs faster in practice compared to these baselines. However, a key limitation of Algorithm 1 is that it requires the explicit calculation of attention weights, making it incompatible with memory-efficient mechanisms like FlashAttention [7]. We address this issue by introducing another fine-tuning method below.

2.3.2 Targeted Fine-tuning of Hallucination Heads

In this section, we propose a targeted fine-tuning method (Algorithm 2 in the Appendix) to mitigate hallucination by addressing hallucination-prone attention heads in LVLMs, ensuring strong performance with greedy decoding. Our training objective combines next-token prediction for quality and a

[3] We provide an explanation Appendix D.2. We examine the linear spaces spanned by feature representations of text tokens and image tokens, respectively. We find that some directions in the text space cannot be represented by the image space, so changing image attention weights is not sufficient.

Table 1: Hallucination rates in terms of CHAIR_S and CHAIR_I on COCO and Nocaps (Out-of-Domain) image captioning tasks, with lower value indicating better performance.

Methods	COCO				Nocaps (Out-of-Domain)			
	LLaVA-7B		MiniGPT-4		LLaVA-7B		MiniGPT-4	
	CHAIR_S	CHAIR_I	CHAIR_S	CHAIR_I	CHAIR_S	CHAIR_I	CHAIR_S	CHAIR_I
Greedy	51.8	13.3	40.6	13.7	43.2	14.3	57.4	20.0
DoLA	53.8	13.9	41.0	13.8	42.0	13.7	57.2	20.4
OPERA	50.2	14.5	35.2	12.8	44.2	14.4	$\underline{46.2}$	$\underline{16.2}$
VCD	55.4	15.7	38.8	14.8	43.6	14.4	48.2	17.5
LURE	51.2	13.4	46.4	14.2	41.8	14.4	55.8	19.6
HALC	50.2	12.4	36.4	11.8	40.2	12.2	53.0	18.0
AD-HH (Ours)	**29.6**	**8.0**	$\underline{35.2}$	$\underline{11.7}$	$\underline{35.6}$	**9.4**	46.8	**16.2**
TF-HH (Ours)	$\underline{35.0}$	$\underline{8.7}$	**32.0**	**11.4**	**35.4**	$\underline{11.1}$	**45.2**	16.8

text-attention penalty to reduce hallucinations. For a training sample $(v, x, y_{1:T})$, we define the loss:

$$\mathcal{L}(v, x, y_{1:T}) = \sum_{t=1}^{T} \left[\underbrace{-\log P_M(y_t | v, x, y_{<t})}_{\text{next-token-prediction}} + \lambda \sum_{h \in \mathcal{H}_{\text{hallucination}}} \underbrace{\log A_h^{\text{text}}(v, x, y_{<t})}_{\text{text-reliance-reduction}} \right], \tag{3}$$

where $\lambda > 0$ controls the text-reliance penalty. We fine-tune only the hallucination heads and the language model's final prediction layer, achieving significant improvements with minimal compute—200 optimization steps for LLaVA-7B required less than 3% of the compute for instruction tuning.

3 Experiments

In addition to the previously examined LLaVA-7B model, we also investigate the well-known LVLM model MiniGPT-4 [31], which has 7B parameters as LLaVA.

Baselines. Alongside proposed methods for mitigating hallucination, we also study baseline approaches from prior literature, including the standard greedy decoding method and several state-of-the-art techniques: OPERA [11], VCD [12], LURE [30], and HALC [5]. Additionally, we include DoLA [6], which was originally designed to enhance factuality in language models and has also been studied in previous literature. Hyper-parameters of these baselines follow from previous literature and are provided in Appendix E for reference.

Dataset. We focus on hallucination in open-ended generation tasks to assess the effectiveness of our methods. To evaluate object hallucination in visual caption, we use images from the COCO validation and Nocaps [1] datasets. For Nocaps, we use the out-of-domain version. We randomly select 500 samples from each and prompt the LVLMs with the query, "Please describe this image in detail".

Evaluation Metrics. To evaluate object hallucination in image caption, we employ CHAIR metrics [20], designed for automatic hallucination assessment. CHAIR measures the hallucination rate by computing the proportion of objects mentioned in a generated description that are absent from the ground-truth labels. The metric is split into two components: sentence-level hallucination (CHAIR_S) and image-level hallucination (CHAIR_I).

Main Results. We present the evaluation results on COCO in Table 1 (left). Our methods—either decoding or fine-tuning—achieve consistent improvements for both models, reducing hallucination rates by up to 1.7 times compared to greedy decoding for LLaVA-7B and 1.3 times for MiniGPT-4. We also note that reducing hallucinations does not compromise text generation quality, which is shown in Table 3 in the Appendix D.3. We find that DoLA is ineffective in this scenario, a finding also observed in the HALC paper. This is likely because DoLA is designed to elicit factual knowledge from the model, which may unintentionally amplify language biases inherited from the base language model, making it unsuitable for mitigating hallucinations in LVLMs.

Recall that the hallucination heads in our methods were identified using the COCO training dataset, and the above evaluation is with the COCO validation dataset. To examine the transferability and robustness across datasets, we evaluate performance on the Nocaps (out-of-domain) dataset, which includes objects not present in COCO. We report the results in Table 1 (right). We observe similar conclusions: our method maintains strong performance on out-of-domain datasets, indicating that modifications to the hallucination heads have a broad impact across tasks and implying the generalizability of our method.

References

[1] Harsh Agrawal, Karan Desai, Yufei Wang, Xinlei Chen, Rishabh Jain, Mark Johnson, Dhruv Batra, Devi Parikh, Stefan Lee, and Peter Anderson. Nocaps: Novel object captioning at scale. In *Proceedings of the IEEE/CVF international conference on computer vision*, pages 8948–8957, 2019.

[2] Jinze Bai, Shuai Bai, Shusheng Yang, Shijie Wang, Sinan Tan, Peng Wang, Junyang Lin, Chang Zhou, and Jingren Zhou. Qwen-vl: A versatile vision-language model for understanding, localization, text reading, and beyond. 2023.

[3] Zechen Bai, Pichao Wang, Tianjun Xiao, Tong He, Zongbo Han, Zheng Zhang, and Mike Zheng Shou. Hallucination of multimodal large language models: A survey. *arXiv preprint arXiv:2404.18930*, 2024.

[4] Satanjeev Banerjee and Alon Lavie. Meteor: An automatic metric for mt evaluation with improved correlation with human judgments. In *Proceedings of the acl workshop on intrinsic and extrinsic evaluation measures for machine translation and/or summarization*, pages 65–72, 2005.

[5] Zhaorun Chen, Zhuokai Zhao, Hongyin Luo, Huaxiu Yao, Bo Li, and Jiawei Zhou. Halc: Object hallucination reduction via adaptive focal-contrast decoding. *ICML*, 2024.

[6] Yung-Sung Chuang, Yujia Xie, Hongyin Luo, Yoon Kim, James Glass, and Pengcheng He. Dola: Decoding by contrasting layers improves factuality in large language models. In *ICLR*, 2024.

[7] Tri Dao. Flashattention-2: Faster attention with better parallelism and work partitioning. *arXiv preprint arXiv:2307.08691*, 2023.

[8] Chaoyou Fu, Peixian Chen, Yunhang Shen, Yulei Qin, Mengdan Zhang, Xu Lin, Zhenyu Qiu, Wei Lin, Jinrui Yang, Xiawu Zheng, et al. Mme: a comprehensive evaluation benchmark for multimodal large language models. corr abs/2306.13394 (2023). 2023.

[9] Yossi Gandelsman, Alexei A Efros, and Jacob Steinhardt. Interpreting clip's image representation via text-based decomposition. *arXiv preprint arXiv:2310.05916*, 2023.

[10] Raymond Hicks and Dustin Tingley. Causal mediation analysis. *The Stata Journal*, 11(4):605–619, 2011.

[11] Qidong Huang, Xiaoyi Dong, Pan Zhang, Bin Wang, Conghui He, Jiaqi Wang, Dahua Lin, Weiming Zhang, and Nenghai Yu. Opera: Alleviating hallucination in multi-modal large language models via over-trust penalty and retrospection-allocation. In *Proceedings of the IEEE/CVF Conference on Computer Vision and Pattern Recognition*, pages 13418–13427, 2024.

[12] Sicong Leng, Hang Zhang, Guanzheng Chen, Xin Li, Shijian Lu, Chunyan Miao, and Lidong Bing. Mitigating object hallucinations in large vision-language models through visual contrastive decoding. In *Proceedings of the IEEE/CVF Conference on Computer Vision and Pattern Recognition*, pages 13872–13882, 2024.

[13] Junnan Li, Dongxu Li, Silvio Savarese, and Steven Hoi. Blip-2: Bootstrapping language-image pre-training with frozen image encoders and large language models. In *International conference on machine learning*, pages 19730–19742. PMLR, 2023.

[14] Yifan Li, Yifan Du, Kun Zhou, Jinpeng Wang, Wayne Xin Zhao, and Ji-Rong Wen. Evaluating object hallucination in large vision-language models. *arXiv preprint arXiv:2305.10355*, 2023.

[15] Chin-Yew Lin and FJ Och. Looking for a few good metrics: Rouge and its evaluation. In *Ntcir workshop*, 2004.

[16] Tsung-Yi Lin, Michael Maire, Serge Belongie, James Hays, Pietro Perona, Deva Ramanan, Piotr Dollár, and C Lawrence Zitnick. Microsoft coco: Common objects in context. In *Computer Vision–ECCV 2014: 13th European Conference, Zurich, Switzerland, September 6-12, 2014, Proceedings, Part V 13*, pages 740–755. Springer, 2014.

[17] Haotian Liu, Chunyuan Li, Qingyang Wu, and Yong Jae Lee. Visual instruction tuning. In *Advances in neural information processing systems*, volume 36, 2024.

[18] Catherine Olsson, Nelson Elhage, Neel Nanda, Nicholas Joseph, Nova DasSarma, Tom Henighan, Ben Mann, Amanda Askell, Yuntao Bai, Anna Chen, et al. In-context learning and induction heads. *arXiv preprint arXiv:2209.11895*, 2022.

[19] Alec Radford, Jong Wook Kim, Chris Hallacy, Aditya Ramesh, Gabriel Goh, Sandhini Agarwal, Girish Sastry, Amanda Askell, Pamela Mishkin, Jack Clark, et al. Learning transferable visual models from natural language supervision. In *International conference on machine learning*, pages 8748–8763. PMLR, 2021.

[20] Anna Rohrbach, Lisa Anne Hendricks, Kaylee Burns, Trevor Darrell, and Kate Saenko. Object hallucination in image captioning. *arXiv preprint arXiv:1809.02156*, 2018.

[21] Shengbang Tong, Ellis Brown, Penghao Wu, Sanghyun Woo, Manoj Middepogu, Sai Charitha Akula, Jihan Yang, Shusheng Yang, Adithya Iyer, Xichen Pan, et al. Cambrian-1: A fully open, vision-centric exploration of multimodal llms. *arXiv preprint arXiv:2406.16860*, 2024.

[22] Ashish Vaswani, Noam Shazeer, Niki Parmar, Jakob Uszkoreit, Llion Jones, Aidan N Gomez, Lukasz Kaiser, and Illia Polosukhin. Attention is all you need. *arXiv preprint arXiv:1706.03762*, 10, 2017.

[23] Elena Voita, David Talbot, Fedor Moiseev, Rico Sennrich, and Ivan Titov. Analyzing multi-head self-attention: Specialized heads do the heavy lifting, the rest can be pruned. *arXiv preprint arXiv:1905.09418*, 2019.

[24] Kevin Wang, Alexandre Variengien, Arthur Conmy, Buck Shlegeris, and Jacob Steinhardt. Interpretability in the wild: a circuit for indirect object identification in gpt-2 small. *ICLR*, 2023.

[25] Guangxuan Xiao, Yuandong Tian, Beidi Chen, Song Han, and Mike Lewis. Efficient streaming language models with attention sinks. *arXiv preprint arXiv:2309.17453*, 2023.

[26] Qinan Yu, Jack Merullo, and Ellie Pavlick. Characterizing mechanisms for factual recall in language models. *arXiv preprint arXiv:2310.15910*, 2023.

[27] Weihao Yu, Zhengyuan Yang, Linjie Li, Jianfeng Wang, Kevin Lin, Zicheng Liu, Xinchao Wang, and Lijuan Wang. Mm-vet: Evaluating large multimodal models for integrated capabilities. In *ICML*, 2024.

[28] Muru Zhang, Ofir Press, William Merrill, Alisa Liu, and Noah A Smith. How language model hallucinations can snowball. *arXiv preprint arXiv:2305.13534*, 2023.

[29] Haiyan Zhao, Hanjie Chen, Fan Yang, Ninghao Liu, Huiqi Deng, Hengyi Cai, Shuaiqiang Wang, Dawei Yin, and Mengnan Du. Explainability for large language models: A survey. *ACM Transactions on Intelligent Systems and Technology*, 15(2):1–38, 2024.

[30] Yiyang Zhou, Chenhang Cui, Jaehong Yoon, Linjun Zhang, Zhun Deng, Chelsea Finn, Mohit Bansal, and Huaxiu Yao. Analyzing and mitigating object hallucination in large vision-language models. *ICLR*, 2024.

[31] Deyao Zhu, Jun Chen, Xiaoqian Shen, Xiang Li, and Mohamed Elhoseiny. Minigpt-4: Enhancing vision-language understanding with advanced large language models. *arXiv preprint arXiv:2304.10592*, 2023.

A Related Work

Mitigating Hallucinations in LVLMs. LVLMs' hallcunation behaviors are particularly severe in open-ended generation tasks [11, 30, 28]. Many approaches have been explored to mitigate hallucinations in LVLMs, most of which focus on better decoding strategies. For instance, Leng *et al.* [12] introduced visual contrastive decoding, which compares output distributions from original and distorted visual inputs to correct the model's over-reliance on unimodal priors and statistical bias. Moreover, Huang *et al.* [11] observed that LVLMs frequently depend on the so-called summary tokens and proposed a method combining beam-search with retrospection-allocation, penalizing over-reliance on these tokens. Additionally, Chen *et al.* [5] highlighted the importance of incorporating both local and global visual context, with the HALC method using an external grounding module during decoding. Furthermore, Zhou *et al.* [30] developed LURE, which rectifies text by revising generated content to mitigate hallucination issues like co-occurrence errors and object ambiguity. In contrast to previous studies, our work identifies a module-level cause of hallucination in LVLMs and develops targeted intervention strategies to mitigate hallucination effectively. In addition, a key feature of our method is that it requires only a single generation forward process during decoding, which is faster than existing methods.

Interpretability of Transformers. Understanding and explaining neural networks, particularly Transformers [22], is crucial for identifying their behaviors and limitations [29]. A widely used approach is causal mediation analysis [10], which attributes the contributions of key components, often employing "knock-out" techniques [24] to assess the impact of removing specific model elements on the output. Previous research [23, 18, 26, 9] has demonstrated that individual attention heads in Transformers frequently assume distinct roles, such as induction, copying, and memorization. While prior studies, such as [30], have also explored to understand hallucination in LVLMs, our work approaches it through the attribution of key components and intervenes in them specifically.

B Preliminary

LVLMs usually process both visual and linguistic data using three components: a vision encoder, a connector, and a Large Language Model (LLM). The vision encoder processes visual input, the connector aligns it with text tokens, and the LLM generates responses from this multimodal input. The LLM, structured as a transformer [22], consists of L layers. Each layer includes a Multi-Head Attention (MHA) module and a Multi-Layer Perceptron (MLP), applying two primary residual transformations to the output of the previous layer $Z^{\ell-1}$:

$$\widehat{Z}^{\ell} = \mathrm{MHA}^{\ell}(Z^{\ell-1}) + Z^{\ell-1}, \quad Z^{\ell} = \mathrm{MLP}^{\ell}(\widehat{Z}^{\ell}) + \widehat{Z}^{\ell}.$$

In this framework, a layer ℓ employs an MHA module consisting of H attention heads. Each head executes a self-attention operation, where the attention score is computed using query, key, and value matrices derived from the input. Specifically, for the i-th head in layer ℓ, the operation is given by:

$$\mathrm{head}_i^{\ell}(Z^{\ell-1}) = \mathrm{Attention}(Q_i^{\ell}, K_i^{\ell}, V_i^{\ell}) = \mathrm{softmax}\left(\frac{Q_i^{\ell}(K_i^{\ell})^{\top}}{\sqrt{d_k}}\right) V_i^{\ell},$$

where $Q_i^{\ell} = Z^{\ell-1}W_i^{Q,\ell}$ is the query matrix for the i-th head, and $K_i^{\ell} = Z^{\ell-1}W_i^{K,\ell}$ is the key matrix for the i-th head, and $V_i^{\ell} = Z^{\ell-1}W_i^{V,\ell}$ is the value matrix for the i-th head, and d_k is the dimensionality of the key vectors. The outputs from all H heads are then concatenated and projected using an output projection matrix $W^{O,\ell}$:

$$\mathrm{MHA}^{\ell}(Z^{\ell-1}) = \mathrm{Concat}(\mathrm{head}_1^{\ell}(Z^{\ell-1}), \mathrm{head}_2^{\ell}(Z^{\ell-1}), \ldots, \mathrm{head}_H^{\ell}(Z^{\ell-1}))W^{O,\ell}.$$

For common 7B models such as LLaVA [17] and MiniGPT4 [31], we have $L = 32$ and $H = 32$ and $d_k = 128$.

C Algorithms

Algorithm 1 Adaptive Deactivation of Hallucination Heads (AD-HH)

```
Require: Hallucination Head Set $\mathcal{H}_{\text{hallucination}}$, Threshold $\tau$
for decoding time step $t$ do
    if attention head $h$ in $\mathcal{H}_{\text{hallucination}}$ then
        $I_h^{\text{text}} \leftarrow$ sum of text attention weights
        if $I_h^{\text{text}} > \tau$ then
            Set the text attention weights to zero
        Self-attention calculation
    else
        Self-attention calculation
```

Algorithm 2 Targeted Fine-Tuning of Hallucination Heads (TF-HH)

```
Require: Hallucination Head Set $\mathcal{H}_{\text{hallucination}}$, dataset $\mathcal{D}$
for component $c$ do
    if $c$ in $\mathcal{H}_{\text{hallucination}}$ or $c$ is language head then
        c.requires_grad = true
    else
        c.requires_grad = false
for fine-tuning steps do
    Calculate the loss in Equation (3) for samples in $\mathcal{D}$
    Perform gradient descent update
```

D Additional Results

D.1 Additional Results on Component Attribution

On the importance of contrastive influence metric. To validate the proposed contrastive influence metric, which isolates a head's effect on generating hallucinated versus non-hallucinated objects, we compare it to the non-contrastive influence, i.e., directly use $\mathcal{I}_{h,\text{hallucination}}$ for identifying hallucination heads. In Table 2, we report the evaluation results for LLaVA-7B on the COCO captioning task, where we adaptively deactivate the top-20 hallucination heads identified through contrastive and non-contrastive methods. As shown, deactivating heads identified by contrastive influence results in a significantly greater reduction in hallucinations, highlighting its superior precision in localizing hallucination heads.

Table 2: Ablation study on constrative influence.

Method	CHAIR_S	CHAIR_I
Greedy	51.8	13.3
AD-HH (Non-contrastive Influence)	41.8	11.0
AD-HH (Constrative Influence)	**29.6**	**8.8**

Sensitivity analysis of the causal mediation method. In Figure 6(a), we plot the Spearman rank correlation between the contrastive influence scores of each attention head found using N samples and those using 1000 samples. Here, N represents the number of samples used for hallucination head attribution. Varying N from 50 to 1000, we observe that when N reaches 500, the Spearman rank correlation is 0.93 compared to the results with $N = 1000$. Beyond $N = 500$, increasing the number of samples results in minimal changes to the attribution outcomes. This indicates that 500 samples are sufficient for accurately identifying hallucination heads.

We also evaluate alternative “knock-out" techniques for identifying hallucination heads, including: 1) using log probabilities instead of probabilities for intervention effects, and 2) replacing the output of the target component with the mean value of the hidden state outputs. In Figure 6(b,c), we plot the Pearson correlation between these two alternative methods and our default zero-ablation method using probabilities. The high correlation observed suggests that the intervention results (contrastive influence) of each head align closely with the default methods, indicating that our approach exhibits low sensitivity.

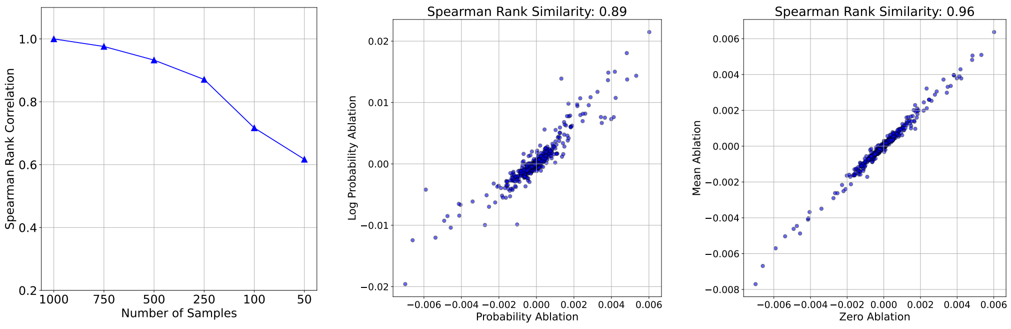

(a) (b) (c)

Figure 6: (a) Ablation study on number of samples to identify hallucination heads. (b) Spearman rank similarity comparison between effects calculated on log probability and probability. (c) Spearman rank similarity comparison between mean-ablation and zero-ablation methods.

Component attribution results on MiniGPT-4. In Figure 7, we present the constrastive influence of attention heads in the MiniGPT-4 model on generating hallucinated and non-hallucinated objects. As indicated in the Figure, the hallucination heads also are distributed in the latter half of the model.

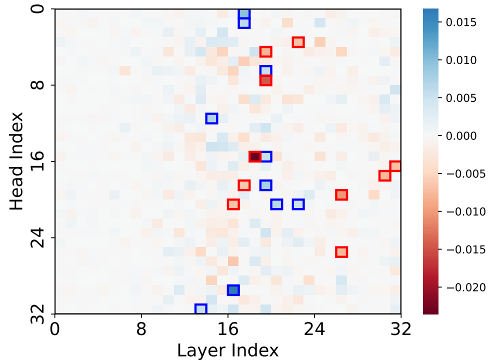

Figure 7: Contrastive influence of attention heads in the MiniGPT-4 model. Bluer box indicate heads more responsible for generating hallucinated objects.

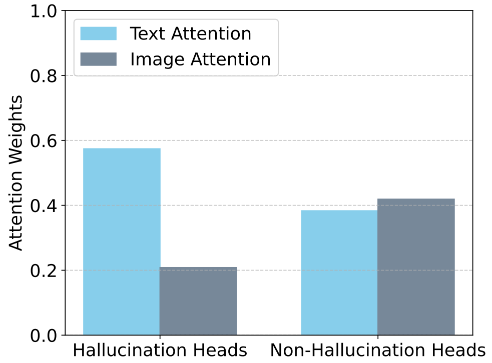

Figure 8: Averaged attention weights on text and image tokens for hallucination and non-hallucination heads identified in MiniGPT-4.

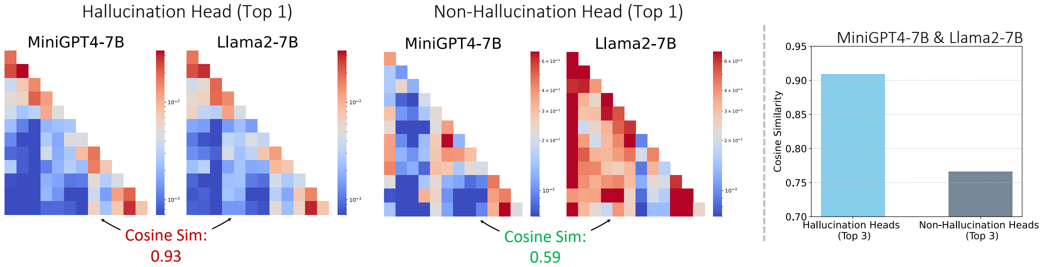

Figure 9: Hallucination heads in MiniGPT-4 inherit the text attention pattern from the base LLM.

D.2 Additional Results on Behaviour Analysis of Hallucination Heads

Some Hallucination Heads Show Slow Changes in Attention Maps During Visual Instruction Tuning. The above results imply that hallucination heads likely inherit much of their behavior from the base language model, despite undergoing extensive visual instruction tuning (e.g., 665k samples for LLaVA-7B). To provide further evidence for this, we replicate the visual instruction tuning process of LLaVA-7B and calculate the Jensen-Shannon (JS) divergence between the attention maps before and after tuning. As shown in Figure 10, we find that top hallucination heads are “lazy", displaying noticeably slower changes in attention maps compared to non-hallucination heads. This insight could be valuable for the future development of LVLMs and warrants further investigation. For our work, this finding motivates the design of targeted fine-tuning strategies, rather than full-parameter tuning, to mitigate hallucinations in the next section.

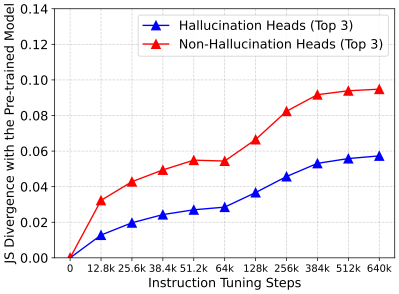

Figure 10: JS divergence of the attention map from the initial model (before visual instruction tuning) throughout the tuning process.

Attention bias of hallucination heads in MiniGPT-4. In Figure 8, we plot the averaged attention weights on text and image tokens for top-3 hallucination and non-hallucination heads. As shown in the Figure, the hallucination heads of MiniGPT-4 also demonstrate much stronger attention bias than non-hallucination heads.

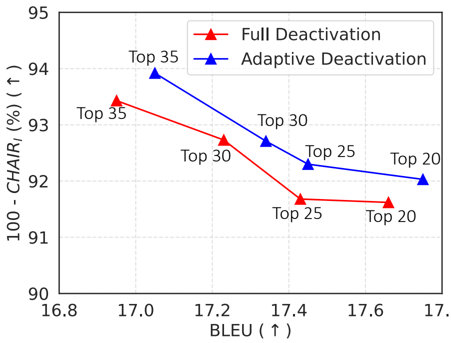

Figure 11: Compare adaptive deactivation and full deactivation in reducing hallucination and maintaining generation quality.

Table 3: Generation quality comparison, with higher value indicating better performance.

Dataset	COCO			Nocaps		
	BLEU	ROUGH	METEOR	BLEU	ROUGH	METEOR
Greedy	17.9	18.8	18.2	24.6	21.8	18.8
AD-HH (Ours)	17.8	19.1	18.1	23.1	21.3	18.3
TF-HH (Ours)	**18.8**	**20.0**	**18.7**	**25.5**	**22.9**	**19.2**

Inherited attention pattern of hallucination heads in MiniGPT-4. In Figure 9, we compare the attention patterns of hallucination heads in MiniGPT-4 with those in its base language model, Llama-2-7B. As shown, the text attention patterns in MiniGPT-4 are more aligned with Llama-2-7B for hallucination heads than for non-hallucination heads. Specifically, the top hallucination head with the highest contrastive influence shows a cosine similarity as high as 0.93, in contrast to the top non-hallucination head, which only exhibits a similarity of 0.59.

Spanned linear space analysis. Our findings in Section 2.3 indicate that downscaling text attention weights is more effective than upscaling image attention weights. We hypothesize that this can be explained by the linear spaces spanned by text tokens and image tokens. If the space spanned by text tokens is significantly larger than that of image tokens, simply adjusting image attention weights (i.e., modifying the linear combination in the self-attention mechanism) may be insufficient.

To test this, we construct a linear space for text tokens, denoted as $\mathcal{S}_{\text{text}}$, and a linear space for image tokens, denoted as $\mathcal{S}_{\text{image}}$. We then calculate the projection distances:

$$d(\text{projection } \mathcal{S}_{\text{image}} \text{ onto } \mathcal{S}_{\text{text}}) = \|\mathcal{S}_{\text{text}}(\mathcal{S}_{\text{text}}^\top \mathcal{S}_{\text{text}})^{-1}\mathcal{S}_{\text{text}}^\top \mathcal{S}_{\text{image}}\|_F = 3636.3$$

$$d(\text{projection } \mathcal{S}_{\text{text}} \text{ onto } \mathcal{S}_{\text{image}}) = \|\mathcal{S}_{\text{image}}(\mathcal{S}_{\text{image}}^\top \mathcal{S}_{\text{image}})^{-1}\mathcal{S}_{\text{image}}^\top \mathcal{S}_{\text{text}}\|_F = 15688.5$$

The results suggest that certain directions in the text space cannot be linearly represented by the image token features. As a result, even with careful tuning of image attention weights, the output of the self-attention mechanism may still retain components of textual information, contributing to hallucination.

D.3 Additional Results on Modular Intervention

On the effectiveness of adaptive deactivation. To illustrate the effectiveness of adaptive deactivation of hallucination heads in preserving the generation quality and mitigating hallucination, we compare the performance of our proposed adaptive deactivation method and full deactivation, which completely setting the text attention weights of hallucination heads to zero regardless of the input. Figure 11 shows the the hallucination rate (CHAIR_{I}) and generation quality (BLEU) of the two methods as the number of top-k hallucination heads to be deactivated varied. As illustrated in the Figure, adaptive deactivation yeilds more optimal hallucination reduction and generation quality maintaining with the same number of top-k hallucination heads to be deactivated. This indicates that context-aware pruning is more flexible than static pruning method.

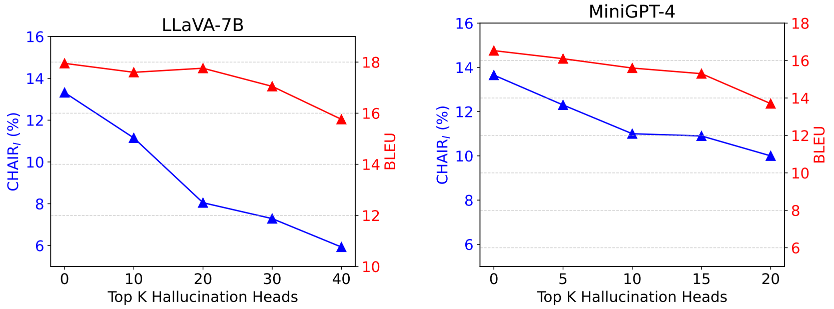

Figure 12: Ablation study on the top-k hallucination head selection.

Table 4: Ablation study on fine-tuned components.

Methods	CHAIR$_S$	CHAIR$_I$
Original Model	51.8	13.3
Fine-tune Full Parameters	56.3	15.6
Fine-tune Random Heads	54.4	15.7
Fine-tune Hallucination Heads	**35.0**	**8.7**

Table 5: Results on the MME dataset.

Method	Score
Greedy	1791.64
AD-HH (Ours)	1812.36
TF-HH (Ours)	**1813.06**

On the top-k hallucination head selection. In Figure 12, we present the relationship between the hallucination rate (CHAIR$_I$) and generation quality (BLEU) as the number k of deactivated hallucination heads increases. As illustrated, increasing k leads to more effective hallucination reduction but is also associated with a decline in generation quality after a certain number of deactivated hallucination heads. We find that for LLaVA-7B, $k = 20$ yields a favorable trade-off between generation quality and hallucination reduction for LLaVA-1.5, while $k = 10$ is optimal for MiniGPT4, which we adopt as our default parameter in adaptive deactivation of hallucination heads.

On the importance of fine-tuning hallucination heads. To highlight the importance of targeting only hallucination heads, we compare the results in Table 4 for fine-tuning the full parameters, 30 randomly selected heads, and the top 30 hallucination heads on LLaVA-1.5. As shown in the table, fine-tuning only the hallucination heads achieves significantly more hallucination reduction compared to both full fine-tuning and fine-tuning random heads. This verifies that hallucination is mainly caused by only a small portion (less than 3%) of attention heads, and focusing on them is crucial for reducing hallucination.

On the generation quality comparison. In Table 11 and Table 12, we visualize some image description examples of the LLaVA-7B model. The hallucinated objects are highlighted in RED. The main results show that our method does not influences the the coherent and fluency of generated context. We qualitatively measure the generation quality in Table 3. For BLEU, ROUGH [15], and METEOR [4], the adaptive deactivation method shows a slight decrease on the Nocaps dataset. While the fine-tuning method maintains and even improve the quality, which indicates that fine-tuning provides a more robust and safe adjustment to the model.

Evaluation on the MME dataset. We also evaluate on the MME benchmark [8], which measures the perception and cognition abilities of LVLMs. As demonstrated in Table 5, our two methods show generalization ability on the benchmark, improving the overall score by about 20 absolute points.

Table 6: Performance in complicated multimodal tasks from MM-Vet [27], with higher value indicating better performance.

Methods	LLaVA-7B							MiniGPT-4						
	Rec	OCR	Know	Gen	Spat	Math	Total	Rec	OCR	Know	Gen	Spat	Math	Total
Greedy	36.3	21.8	17.0	18.9	24.8	7.7	31.4	26.5	13.3	17.5	13.9	22.3	8.1	22.2
DoLA	37.2	22.1	17.9	21.0	26.3	7.7	31.7	24.9	12.9	18.5	12.0	21.7	7.7	21.6
OPERA	35.4	25.6	20.5	**22.9**	**30.9**	**11.5**	32.0	28.2	15.0	16.5	11.4	21.9	11.5	23.6
VCD	33.0	23.6	16.0	19.4	25.6	3.8	29.4	25.3	14.8	17.4	15.0	20.3	0.0	20.9
HALC	36.2	21.5	17.5	20.1	23.5	7.7	30.8	24.9	15.7	15.2	10.7	23.2	7.7	21.7
AD-HH (Ours)	**38.4**	**26.0**	**21.2**	21.9	30.3	7.7	**34.3**	28.2	16.6	16.1	13.7	26.1	12.0	23.8
TF-HH (Ours)	36.6	24.1	17.9	19.0	27.2	**11.5**	32.5	**31.9**	**18.1**	**22.3**	**16.6**	**26.5**	**18.5**	**27.3**

D.4 Additional Results on Hallucination Mitigation Evaluation.

Case Studies. To illustrate the effectiveness of our methods, we present case studies in Figure 13. The original model demonstrates a strong reliance on text tokens, which leads to the generation of hallucination objects that have close semantic relationships with the focus token. We then provide the same prompt before the hallucinated token to our fine-tuned model. We can observe that the fine-tuned model shifts attention more towards the image tokens, resulting in the generation of image-consistent objects.

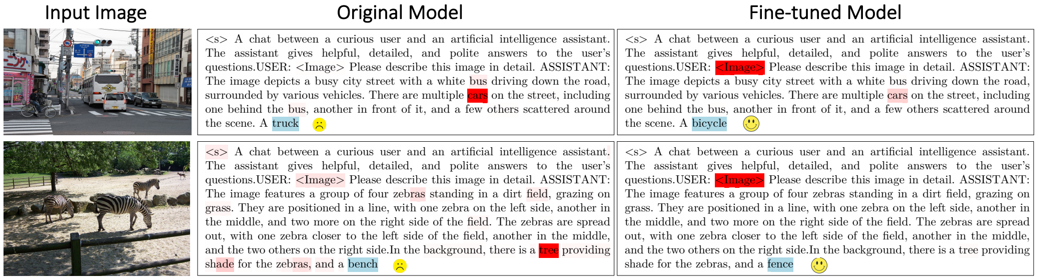

<s> A chat between a curious user and an artificial intelligence assistant. The assistant gives helpful, detailed, and polite answers to the user's questions.USER: <Image> Please describe this image in detail. ASSISTANT: The image depicts a busy city street with a white bus driving down the road, surrounded by various vehicles. There are multiple cars on the street, including one behind the bus, another in front of it, and a few others scattered around the scene. A truck ☹

<s> A chat between a curious user and an artificial intelligence assistant. The assistant gives helpful, detailed, and polite answers to the user's questions.USER: <Image> Please describe this image in detail. ASSISTANT: The image depicts a busy city street with a white bus driving down the road, surrounded by various vehicles. There are multiple cars on the street, including one behind the bus, another in front of it, and a few others scattered around the scene. A bicycle ☺

<s> A chat between a curious user and an artificial intelligence assistant. The assistant gives helpful, detailed, and polite answers to the user's questions.USER: <Image> Please describe this image in detail. ASSISTANT: The image features a group of four zebras standing in a dirt field, grazing on grass. They are positioned in a line, with one zebra on the left side, another in the middle, and two more on the right side of the field. The zebras are spread out, with one zebra closer to the left side of the field, another in the middle, and the two others on the right side.In the background, there is a tree providing shade for the zebras, and a bench ☹

<s> A chat between a curious user and an artificial intelligence assistant. The assistant gives helpful, detailed, and polite answers to the user's questions.USER: <Image> Please describe this image in detail. ASSISTANT: The image features a group of four zebras standing in a dirt field, grazing on grass. They are positioned in a line, with one zebra on the left side, another in the middle, and two more on the right side of the field. The zebras are spread out, with one zebra closer to the left side of the field, another in the middle, and the two others on the right side.In the background, there is a tree providing shade for the zebras, and a fence ☺

Figure 13: Visualization of attention weights for the top hallucination head when predicting the next token (shown in blue). We accumulate the attention weights on a total of 576 image tokens into the placeholder <image> to simplify visualization. Redder values in the context indicate larger attention weights. The original LLaVA-7B model significantly relies on the previously generated tokens, resulting in hallucination. Our model through targeted fine-tuning does not have this issue.

Modular Intervention Benefits Complicated Multimodal Tasks. To further validate our method's effectiveness on complex open-ended multimodal tasks, we evaluated performance on the MM-Vet dataset, which assesses six multimodal capabilities: recognition, OCR, knowledge, language generation, spatial awareness, and math. Table 6 shows that our method, either through decoding or fine-tuning, also improves a range of multimodal capacibilites. For instance, our decoding method boosts LLaVA-7B's scores in OCR and spatial awareness by 4.2 and 5.5 points, respectively. Similarly, our fine-tuning method enhances MiniGPT-4's performance in recognition and math, with improvements of 5.4 and 10.4 points. These results demonstrate that modifying hallucination heads benefits not only tasks focused on hallucination reduction but also general multimodal tasks.

Our Method Runs Fast in Generation. We compare the generation time of our decoding method AD-HH with existing decoding-time hallucination mitigation methods in Figure 14. For OPERA and our method that requires explicit attention weights, we use the standard self-attention implementation. For Greedy, DoLA, VCD, and HALC, where explicit attention weights are not needed, we employ Flash-Attention, which is generally faster than standard self-attention. All methods were tested on a single A100-80GB GPU. We observe that our method achieves similar decoding times to greedy decoding. This is because we intervene on the attention weights on-the-fly during the generation process. In contrast, other methods inevitably introduce computational overhead. For instance, VCD requires a double inference process for contrastive decoding, and OPERA requires retrospecting to previous steps when knowledge aggregation happens.

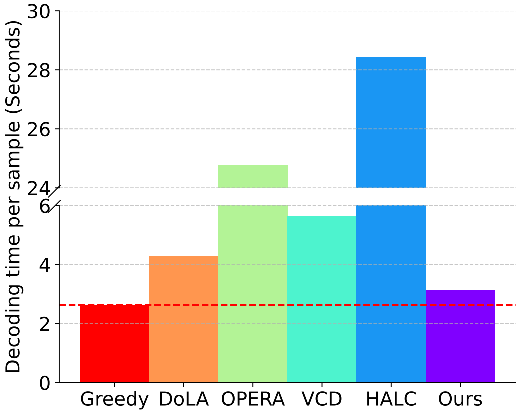

Figure 14: Generation time of a single response.

E Experiment Details

Implementation of Baselines. In Table 7, Table 8, Table 9, and Table 10, we present the hyper-parameters for the baseline methods: DoLA, OPERA, VCD, and HALC. These parameters follow the official configurations provided by their respective sources. For the LURE baseline, we use the MiniGPT-4 13B checkpoint provided in the official repository as the revisor. We observed that, after generating the revised response, LURE's final step involves splitting the response into two parts based on the "\n" symbol and only retaining the first part. However, as most responses generated by LLaVA-7B contain "\n" in the middle, this split function significantly shortens the response length, reducing it by nearly 40% when the maximum generated token length is 128. This could compromise the fairness of the comparison. Therefore, we bypassed this post-processing step and directly used the full output response from the revisor as the final prediction for LURE.

Implementation details of Algorithm 1. We select the top 20 attention heads as hallucination heads for LLaVA-7B and the top 10 heads for MiniGPT-4. For the threshold τ to control the when to deactivate text attention in decoding, we use a sweep search to find an optimal value. Based on this, we set $\tau = 0.4$ for LLaVA-7B and $\tau = 0.5$ for MiniGPT-4.

Implementation details of Algorithm 2. For LLaVA-7B model, we use the instruction-tuning dataset and fine-tuning codes from the offical Github repo[4]. The learning rate is set to 2×10^{-5}, and the global batch size is 128. We fine-tune the model for 200 steps, selecting the top 30 hallucination heads for fine-tuning. For the MiniGPT-4 model, we use the dataset and fine-tuning codes from the offical Github repo[5]. The learning rate is set to 3×10^{-5}, and the global batch size is 128. We fine-tune the model for 200 steps, selecting the top 20 hallucination heads for fine-tuning. For both models, the penalty weight λ is set to 2. We only fine-tune the Query and Key matrices of the attention heads, as this operation modifies how values are linearly combined in self-attention without altering the basis of the linear space. We find that additionally fine-tuning the value matrices is ineffective (i.e., resulting in a higher hallucination rate of CHIRS$_\text{I}$ at 20.86% on LLaVA-7B and lower generation quality). We conjecture that this is because fine-tuning the value matrices significantly disrupts the linear space of the original model.

[4] https://github.com/haotian-liu/LLaVA?tab=readme-ov-file

[5] https://github.com/Vision-CAIR/MiniGPT-4

Table 7: DoLA Hyperparameters.

Parameters	**Value**
Adaptive Plausibility Threshold	0.1
Early Exist Layers	$[0, 2, 4, \cdots, 32]$

Table 8: OPERA Hyperparameters.

Parameters	**Value**
Self-attention Weight Scale Factor	50
Attending Retrospection Threshold	15
Beam Size	5
Penalty Weights	1.0

Table 9: VCD Hyperparameters.

Parameters	**Value**
Amplification Factor	1
Adaptive Plausibility Threshold	0.1
Diffusion Noise Step	500

Table 10: HALC Hyperparameters.

Parameters	**Value**
Detector	Dino
JSD Buffer Size m	6
Beam Size	1
Number of Sampled FOVs n	4
Exponential Ratio of Growiing Contextual Field	0.6
Bounding Box Threshold for Dino	0.4
Adaptive Plausibility Threshold	0.1

Table 11: Generated images description examples.

	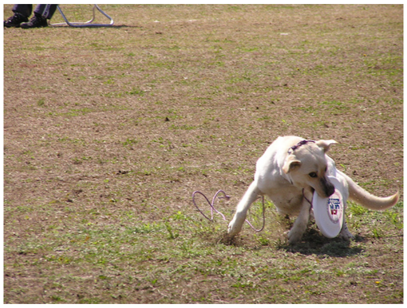
Instruction	Please describe this image in detail.
Greedy	The image features a white dog playing with a frisbee in a grassy field. The dog is holding the frisbee in its mouth, running and enjoying the game. The frisbee is positioned towards the right side of the dog, and the dog appears to be in the middle of the field. \n\n In the background, there is a bench located on the left side of the field, possibly for spectators to sit and watch the dog play.
AD-HH (Ours)	The image features a white dog playing with a frisbee in a grassy field. The dog is holding the frisbee in its mouth, running and playing with the frisbee in the field. The dog appears to be enjoying the game and is actively engaged in the activity.
TF-HH (Ours)	The image features a white dog playing with a frisbee in a field. The dog is in the process of catching the frisbee, which is positioned in the middle of the scene. The dog is running towards the frisbee, displaying its agility and excitement. \n\n The field is spacious, providing ample room for the dog to play and enjoy its frisbee game. The dog's enthusiasm and the frisbee's position in the air create a lively and engaging scene.
	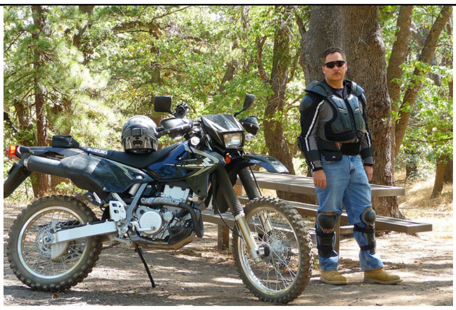
Instruction	Please describe this image in detail.
Greedy	The image features a man standing next to a parked motorcycle, which is prominently displayed in the scene. The man is wearing a helmet and appears to be the owner of the motorcycle. The motorcycle is positioned in the foreground, occupying a significant portion of the image.\n\n In the background, there is a bench situated near the motorcycle, providing a place for the man to sit and relax. The scene also includes a backpack placed on the ground, possibly belonging to the man or someone else in the area.
AD-HH (Ours)	The image features a man standing next to a parked motorcycle, which is parked on a dirt road. The man is wearing a helmet and appears to be the owner of the motorcycle. The motorcycle is positioned on the left side of the image, with the man standing on the right side.\n\n In addition to the motorcycle, there is a bench located in the background, providing a place for the man to rest or take a break. The scene appears to be set in a wooded area, with trees surrounding the area.
TF-HH (Ours)	The image features a man standing next to a parked motorcycle, wearing a black jacket and sunglasses. He is posing for the camera, possibly in a wooded area. The motorcycle is parked on the side of the road, and the man is standing close to it.\n\n There are several trees in the background, and a bench can be seen further back in the scene. The man appears to be the main focus of the image, with the motorcycle and the surrounding environment serving as the backdrop.

Table 12: Generated images description examples.

	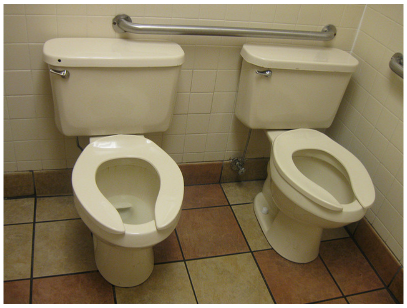
Instruction	Please describe this image in detail.
Greedy	The image features a bathroom with two toilets placed side by side. Both toilets are white and have their lids up, revealing their bowls. The toilets are positioned close to each other, with one slightly closer to the left side of the room and the other slightly closer to the right side.\n\nThe bathroom also contains a sink, which is located towards the left side of the room. The sink is accompanied by a mirror, which is placed above it. The overall scene gives the impression of a public restroom or a shared bathroom space.
AD-HH (Ours)	The image features a bathroom with two toilets placed side by side in a bathroom stall. Both toilets are white and appear to be in good condition. The toilets are positioned close to each other, with one toilet slightly closer to the left side of the bathroom and the other toilet slightly closer to the right side.\n\nThe bathroom appears to be clean and well-maintained, with the toilets being the main focus of the image. The bathroom stall appears to be a public restroom, as it is designed to accommodate multiple users at.
TF-HH (Ours)	The image features a bathroom with two toilets placed side by side. Both toilets are white and appear to be in good condition. One of the toilets is positioned closer to the left side of the image, while the other is situated more towards the right side. \n\n The bathroom also features a tiled floor, which adds to the overall clean and well-maintained appearance of the space.
	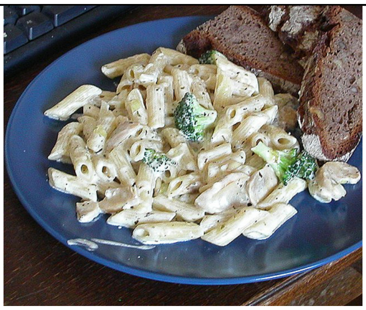
Instruction	Please describe this image in detail.
Greedy	The image features a blue plate filled with a delicious meal consisting of pasta and broccoli. The pasta is mixed with a creamy sauce, and the broccoli pieces are scattered throughout the dish. The plate is placed on a dining table, and there is a sandwich on the table as well. \n\nIn addition to the main dish, there are two bowls in the scene, one located near the top left corner and the other near the top right corner. A keyboard can be seen in the background, suggesting that the dining area is part of a home office or work
AD-HH (Ours)	The image features a blue plate filled with a delicious meal consisting of pasta and broccoli. The plate is placed on a dining table, and the plate is filled with a generous portion of pasta and broccoli. The pasta appears to be a mix of macaroni and shells, and the broccoli is scattered throughout the dish.\n\nIn addition to the main dish, there is a slice of bread on the table, likely to be used as a side or to accompany the meal. The dining table occupies most of the image, and the dining
TF-HH (Ours)	The image features a blue plate filled with a delicious meal consisting of pasta and broccoli. The plate is placed on a wooden table, and the dish is accompanied by a piece of bread. The pasta and broccoli are arranged in a visually appealing manner, creating a colorful and appetizing presentation. The dish appears to be a healthy and nutritious meal, perfect for a meal or a light lunch.